Dynamic gain scheduled control of a Hawk scale model

T. Richardson, M. Lowenberg, C. Jones and A. Dubs
Department of Aerospace Engineering,
University of Bristol
Bristol, UK

ABSTRACT

When designing flight control laws using linearisations of an aircraft model about different flight conditions, some form of scheduling of the resultant gains will often be required to implement the controller over wide operating regions. In practice, the controller gains are often scheduled against relatively slowly-varying system states such as altitude or velocity. However, it may also be desirable to schedule gains against rapidly-varying states such as angle-of-attack, thereby generating a cyclic dependence through hidden coupling terms. Previous published work at Bristol has developed a numerical method of accounting for this dependence when scheduling state feedback gains against coupled states. The resulting `dynamic gain schedule' is shown to significantly improve the transient response of the aircraft model during rapid manoeuvring and to reduce the chances of control surface actuator position limit saturation. In this paper, the novel design process, using eigenstructure assignment, is applied to a mathematical second-order longitudinal aircraft model which represents an approximate BAe Hawk wind-tunnel model. The dynamic gain scheduled controller is shown to work extremely well in practice when applied to the closed-loop experimental rig. Despite the highly nonlinear characteristics of the model aerodynamics and tailplane actuation system, as well as unmodelled high turbulence levels, dynamic gain scheduling demonstrates stable closed loop control even in regions where the nonlinearities are such that conventional gain scheduling fails to produce a stable response.

NOMENCLATURE

Symbols

$\mathbf{A}$	state matrix
$\mathbf{A}_{cl}$	closed-loop state matrix
$\mathbf{B}$	input matrix
I_{yy}	moment of inertia about y-body axis
$\mathbf{K}$	feedback (static) gain matrix
m	aircraft mass
M	aerodynamic pitching moment
q	pitch rate
$\mathbf{u}$	control input
V_t	total translational velocity
$\mathbf{V}$	achievable closed-loop eigenvalues
$\mathbf{x}$	state vector
Z_w	z-wind axis aerodynamic force

Abbreviations

CGS	conventional gain schedule
DGS	dynamic gain schedule

Greek letters

α	angle-of-attack

Paper No. 3158. Manuscript received 12 January 2007, revised 30 March 2007, accepted 3 May 2007.

https://doi.org/10.1017/S0001924000004723 Published online by Cambridge University Press

δ	vector of input parameters
η	tailplane angle
η_{dem}	demanded tailplane angle
$\mathbf{\Lambda}$	desired closed-loop eigenvalues
$\boldsymbol{\phi}$	feedback (dynamic) gain matrix
θ	pitch angle
θ_{dem}	demanded pitch angle
μ	continuation parameter

1.0 INTRODUCTION

The term 'gain scheduling' encompasses a broad range of control strategies[1]. For the purposes of this paper, gain scheduling is defined as the process of sub-dividing a nonlinear control problem into a series of linear ones, design of controllers to suit each linear design condition and then reconstruction of the resultant discrete solutions into a single continuous controller.

Classical gain scheduled (CGS) controllers are generally restricted by a 'slow variation' condition which means that the designed stability is only maintained if the system moves relatively slowly between operating points. The method developed in previous work[2,3] and applied experimentally in this paper addresses this issue. A controller is designed which allows the scheduling variable to be one of the system states. This is achieved via a simple yet effective transformation to take into account the gradient of the final scheduled gains in order to remove the 'hidden coupling terms' identified in the papers by Rugh and Nichols[1,4].

The resulting dynamic gain scheduling (DGS) also ensures that the controller gains are set closer to the current state of the system and therefore provide a response that is close to the desired ideal when moving rapidly between trim conditions. This is achieved by finding nonlinear functions of single states which satisfy closed-loop stability and response requirements on desired equilibrium branches.

Previous work carried out at Bristol into dynamic gain scheduled controllers presented in[2,3,5,6] has only involved theoretical results and numerical models. In this paper, the method has been applied to a Hawk dynamic test rig and the experimental results presented clearly demonstrate the advantages of applying DGS to a real system. The advantages of DGS over CGS have been highlighted in previous work but are shown to carry through to the results generated by a real closed-loop control system and the inherent associated unmodelled dynamics, disturbances and modelling errors.

Sections 2 outlines the eigenstructure assignment used and the design method for dynamic gain scheduling against a single state. Section 3 describes the wind tunnel test set-up along with the aircraft model being used, an approximate 1/16 scale BAe Hawk model. The mathematical model is described in Section 4 and open-loop behaviour of the wind tunnel model is given in Section 5. The design of a classical gain scheduled controller using eigenstructure assignment follows and a corresponding dynamic gain schedule is given. In Section 6 wind tunnel results are presented that compare the response of the closed-loop model to a series of step inputs. Conclusions are given in the final Section 7.

2.0 CLASSICAL GAIN SCHEDULING DESIGN

The basis of this methodology has been presented previously in Ref. 2 but is included here for clarity. Where relevant, notes are given which relate to the application of this theory to the nonlinear Hawk aircraft model. Consider the nonlinear system:

$$\dot{\boldsymbol{x}} = \boldsymbol{f}(\boldsymbol{x},\delta) \qquad \ldots (1)$$

where: $x \in \Re^n$ is the system state vector
$\delta \to \Re^p$ is a vector of parameters
$f : \Re^{n+p} \to \Re^n$ is a smooth nonlinear function

Adding a nonlinear controller to the system and fixing all parameters except one, μ, we have the affine system:

$$\dot{\mathbf{x}} = \boldsymbol{f}(\boldsymbol{x},\mu) + \boldsymbol{g}(\boldsymbol{x},\mu)\boldsymbol{u} \qquad \ldots (2)$$

where: $\boldsymbol{u} \in \Re^m$ is a vector of inputs
$\boldsymbol{f} : \Re^{n+1} \to \Re^n$ is a smooth nonlinear function
$\boldsymbol{g} : \Re^{n+1} \to \Re^n$ is a smooth nonlinear function

Linearising with μ fixed and where $\hat{\mathbf{x}}$ and $\hat{\mathbf{u}}$ are perturbations from the linearisation point gives the equation:

$$\dot{\hat{\mathbf{x}}} = \mathbf{A}\hat{\mathbf{x}} + \mathbf{B}\hat{\mathbf{u}} \qquad \ldots (3)$$

If a state feedback scheme is considered then the input $\mathbf{u}$ is expressed in terms of the states $\mathbf{x}$ and an appropriate feedback gain matrix $\mathbf{K}$. This results in the closed-loop system:

$$\dot{\hat{\mathbf{x}}} = \mathbf{A}\hat{\mathbf{x}} + \mathbf{B}\mathbf{K}\hat{\mathbf{x}} = \mathbf{A}_{\mathbf{cl}}\hat{\mathbf{x}} \qquad \ldots (4)$$

Using this linearisation, the gain matrix can be calculated using a linear design method such as eigenstructure assignment[7-9]. It should be noted that eigenstructure assignment is not the only method that can be used to generate the closed-loop system gain variations. Dynamic gain scheduling has been successfully applied to systems where other methods, such as LQR, have been used to generate the initial gain schedules[10]. The eigenvalues and eigenvectors are related to the closed-loop matrix by:

$$\mathbf{A}_{\mathbf{cl}}\mathbf{V} = \Lambda\mathbf{V} \qquad \ldots (5)$$

where Λ is a matrix that has the closed-loop eigenvalues on the principal diagonal and the achievable closed-loop eigenvectors are given in the modal matrix, $\mathbf{V}$.

It is not possible to simply specify and achieve any set of eigenvalues and eigenvectors — this is dependent on the number of feedback states that are available and the number of control inputs. The number of inputs tends to be much less than the number of states, hence it is usually only possible to define a desired eigenvector which consists of the elements given in Table 1. These are then used to calculate a set of achievable eigenvectors, $\mathbf{V}$.

The feedback gain matrix is calculated via Equation (6) whose derivation is given in Ref. 10 :

$$\mathbf{K} = \mathbf{Z}_{\mathbf{B}}^{-1}\mathbf{U}_{\mathbf{0}}^{\mathbf{T}}\left(\mathbf{V}\Lambda - \mathbf{A}\mathbf{V}\right)\mathbf{V}^{-1} \qquad \ldots (6)$$

where $\mathbf{Z}_{\mathbf{B}}$ and $\mathbf{U}_0$ are obtained via a QR decomposition of the control matrix, $\mathbf{B}$. Hence the parameters that are required in order to calculate $\mathbf{K}$ are the state matrix $\mathbf{A}$, the input matrix $\mathbf{B}$ (and hence $\mathbf{Z}_{\mathbf{B}}$ and $\mathbf{U}_0$), desired eigenvalues $\mathbf{L}$ and the achievable eigenvectors in the modal matrix $\mathbf{V}$. In multi-degree-of-freedom systems with multiple inputs, it is possible to use eigenstructure assignment to achieve, not only desired pole placement, but to shape the response of each mode and achieve, for example, decoupling of longitudinal and lateral aircraft modes.

Table 1
Desired eigenvector elements

Element	Required effect of the state
0	no effect in the mode
1	dominant in the mode
x	left unspecified: allows the unconstrained influence of the element in the mode

https://doi.org/10.1017/S0001924000004723 Published online by Cambridge University Press

In general, with a highly nonlinear vehicle, this linearisation is carried out at multiple points in state space. Thus, a series of parameterised gain matrices is calculated. Note that the required gains may vary considerably over the state-space region of interest and so scheduling of the gain matrices may be necessary to maintain an acceptable control performance. This is indeed the case for the Hawk wind tunnel model, which demonstrates highly nonlinear behaviour over a wide angle-of-attack range. Fixed-gain controllers designed at low to moderate angles of attack lead to undesirable, including unstable, dynamic behaviour at high angles of attack.

It is possible to schedule these 'classical' gains against either μ or $\mathbf{x}$. Scheduling against $\mathbf{x}$ leads to a problem. The gain matrix $\mathbf{K}$ is calculated assuming constant gains at each linearisation and sufficiently slow state variations. However, in the presence of rapid state variations, gain scheduling against system states introduces unwanted additional dynamics or 'hidden coupling terms'. The background and theory that provides the link between CGS and DGS has been explained in several papers including Refs 3 and 6 and therefore, only the main results will be included here for brevity.

2.1 Dynamic gain scheduling

For a parameter-scheduled (static) controller of the form $u = K(\mu)x$ and a state-scheduled (dynamic) controller of the form $u = \phi(x)x$, the gains can be linked by requiring the closed-loop Jacobian matrix to be equivalent. This yields the relationship:

$$K = \frac{\partial \phi}{\partial x} x + \phi(x) \quad \ldots (7)$$

As stated before, it is possible to find K via a controller design process such as eigenstructure assignment (given sufficient control power). To implement a state-scheduled controller, however, $\phi(x)$ is required. This dynamic gain can be found by integrating Equation (7):

$$\int K \mathrm{d}x + c = \phi(x)x \quad \ldots (8)$$

i.e.

$$\phi(x) = \frac{\int K \mathrm{d}x + c}{x} \quad \ldots (9)$$

Therefore, for any first-order system, the closed loop eigenvalue can be placed as desired by using a dynamic gain schedule derived numerically via a transformation from the static gain variation. Furthermore, this can be extended to allow any state that is being fed back, to be scheduled with itself in any higher order system

2.2 Implementation in practice

In practice, K will be determined between a lower x_l and upper x_u limit. Therefore, calculating the definite integral between these two points:

$$\int_{x_l}^{x_u} K \mathrm{d}x = \phi(x_u)x_u - \phi(x_l)x_l \quad \ldots (10)$$

Table 2
Response requirements for the closed-loop Hawk model

Requirement	Value
Scale factor	4
ζ_{sp}	0·707
ω_n	7·07 rad/s
Pole locations	–5±5i

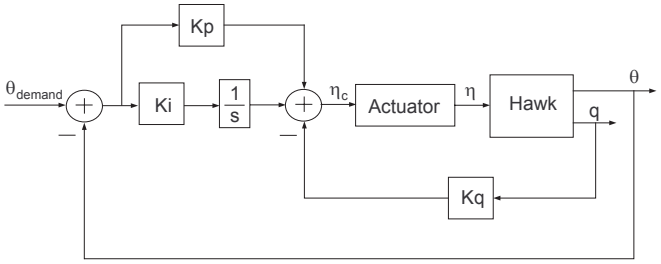


Figure 1. Hawk control law block diagram.

Rearranging the equation for $\phi(x_u)x_u$ results in:

$$\phi(x_u)x_u = \int_{x_l}^{x_u} K \mathrm{d}x + \phi(x_l)x_l \quad \ldots (11)$$

The term $\phi(x_l)x_l$ is a constant and is zero when the integration is started from zero. So, if K has been found numerically then a numerical integration can be used to find $\phi(x)$. The gain schedule given in Section 6 for the Hawk model passes through zero, and hence the transformation is applied from zero. This removes the need to find the constant identified in Equation (11). In the case where the gain is scheduled with a different state, an additional feedback term is introduced on the scheduling state to remove the hidden coupling term. This `modified DGS' is described in full by Jones[6].

2.3 Design criteria scaling

The eigenstructure assignment method requires the eigenvalues to be defined by the user (optimisation methods such as LQR[11] do not require this). Closed-loop eigenvalue pole locations for the short-period mode were chosen in order to just satisfy Level 1 handling qualities requirements for a full-scale aircraft[12]. Subscale models exhibit rotation rates faster than full-sized equivalent vehicles, so the handling qualities parameters were scaled according to angular rate similitude requirements. These are shown in Table 2.

In order to simplify the design, note that one further DGS requirement is that the trim points are identical for the closed-loop static and dynamic scheduled systems. The reason for this is to ensure that the correct gains are applied for the current state of the system. The gain schedules are created for a unique set of trim points and the closed loop gains only create the desired dynamic response when applied at these points. This is achieved for the Hawk model via the use of a command augmentation system (CAS) in pitch which incorporates integral control. Integral control ensures, for the second-order Hawk model, that the closed-loop trim states for the dynamically-scheduled system are identical to those for the classical gain-scheduled system.

2.4 Control law structure

A proportional plus integral (PI) controller with an inner-loop pitch rate compensator controller structure was used (see Fig. 1). The gains were calculated simultaneously by using an eigenstructure assignment routine on linearisations of the mathematical model of the system at trim points across the flight envelope.

The Hawk model experiences a nonlinear variation of pitch damping, leading to instability of the equilibria over part of the operating region. An inner-loop pitch rate compensator controller structure was selected to restore stability and achieve the desired response characteristics and an outer PI loop on pitch angle formed the CAS.

https://doi.org/10.1017/S0001924000004723 Published online by Cambridge University Press



Figure 2. Pendulum support rig (1-DOF) in the 1·1m open-jet wind tunnel.

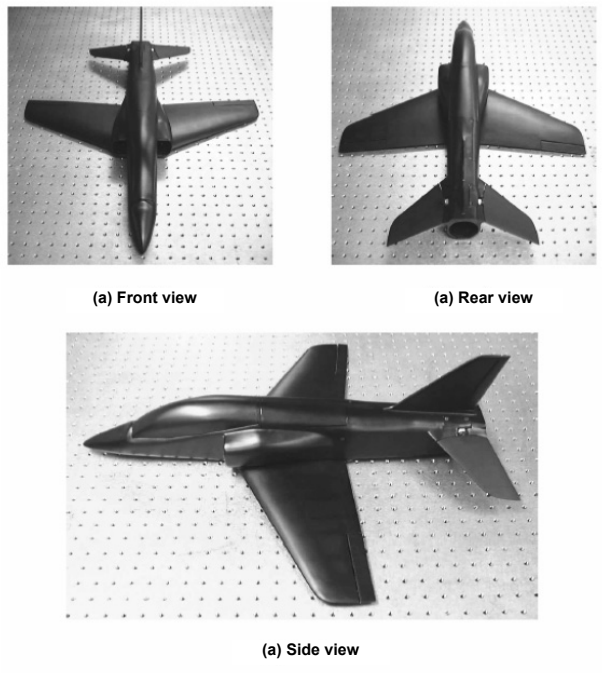


Figure 3. Photographs of the approximate 1/16 scale BAe Hawk.

3.0 HAWK WIND-TUNNEL RIG

This comprises a remotely controlled aircraft model suspended on a gimballed pendulum support strut which allows rotation of the aircraft in pitch (Fig. 2). There are mechanical constraints on the gimbal which could be removed to allow roll and yaw motion[13].

The wind tunnel has a diameter of 1·1m and can provide a maximum speed of 40ms^{-1} with a turbulence level of approximately 1·5% at 20ms^{-1}. All tests were performed at 20ms^{-1} which corresponds to a Reynolds number of $0{\cdot}2\times10^6$, based on the wing chord. The model used for all the tests in this project is an approximate 1/16 scale BAe Hawk, constructed mainly of fibreglass covered wood (Fig. 3). The dimensions, mass of the model without gimbals, as well as approximate moments of inertia of the model, are given in Table 3.

Table 3
Hawk model specifications

Specification	Value
Length	0·655m
Wing span	0·612m
Mean aerodynamic chord	0·135m
Mass	1·8kg
Model inertias	Ixx = 0·00959, Iyy = 0·0395, Izz = 0·0507kgm^2
Servos	5 Supertec Hp/BB
Gimbal potentiometers	Penny and Giles RCP09, range ±90 degrees

3.1 Experimental limitations

The objective of these experiments was not to predict behaviour of, or design a controller for, a specific aircraft using a scale model. Consequently, the standard wind-tunnel testing issues of Reynolds number and Mach number scaling, blockage, boundary and interference effects were not of concern. Instead, the factors that were relevant in this experimental control task were:

- **Time lag and freeplay/backlash at control surfaces**
  Some of these effects are highly nonlinear and thus cannot be modelled as linear systems. Freeplay and backlash are caused by aerodynamic and control linkage loads and friction. This problem could be partially solved if servos with higher torque and better positional accuracy were used.

- **Electrical noise**
  Although the potentiometers have specifications with a high degree of accuracy, their output signal was corrupted by electrical noise from the environment. Furthermore, it was observed that the actuators were affected by electrical interference transmitted through the power supply device from the electrical network.

- **Wind-tunnel turbulence**
  All tests in this project were carried out in the open-jet wind-tunnel. As a result of its short contraction and relatively low contraction ratio, there is a high level of turbulence.

- **Significant nonlinearity in aircraft pitch response**
  The equilibria are stable at low and high angles of attack but at intermediate angles, a large-amplitude limit cycle dominates the response. The aerodynamic nonlinearities are mentioned briefly here but are demonstrated graphically in the open-loop results given in Section 5.

The difficulties arising from these limitations ensured an extremely demanding experimental test for the nonlinear gain-scheduled control systems — in the results discussed here, the principal issues

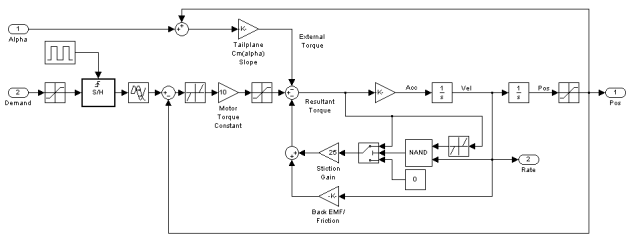


Figure 4. Nonlinear actuator model.

https://doi.org/10.1017/S0001924000004723 Published online by Cambridge University Press

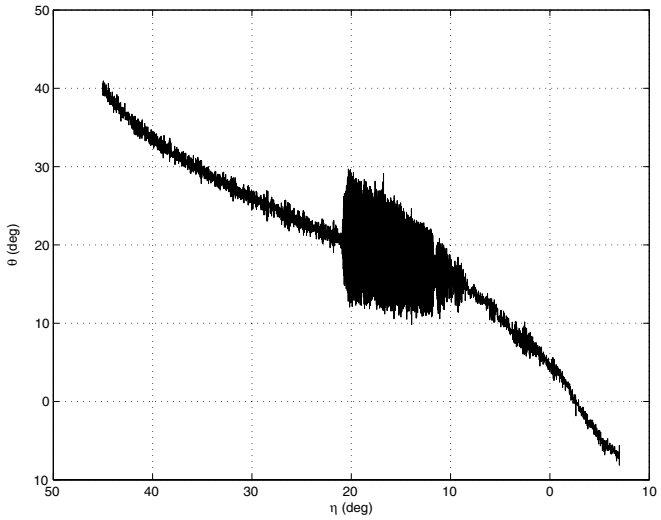


Figure 5. Uncontrolled Hawk: slow tailplane ramp input from +7 to –45 degrees.

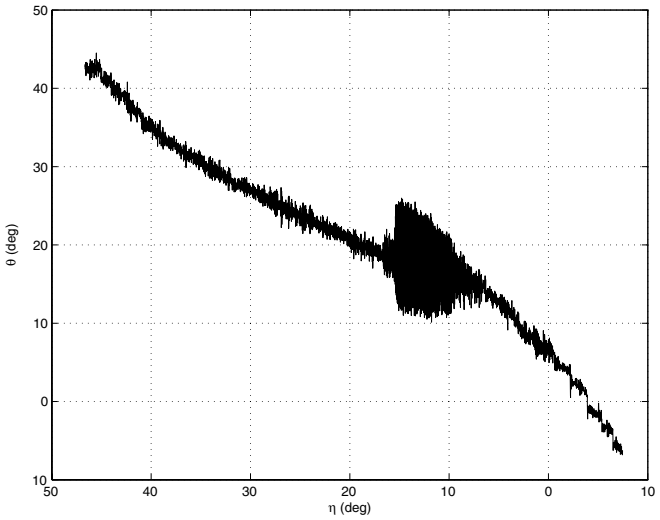


Figure 6. Uncontrolled Hawk: slow tailplane ramp input from –45 to +7 degrees.

were with the turbulence which produced significant model disturbances and with the nonlinear aircraft behaviour in pitch. More details on the wind tunnel model and the nonlinear behaviour demonstrated in multiple degrees of freedom can be found in the references by Kyle[14] and Davison[13].

4.0 THE MATHEMATICAL MODEL

4.1 Second order Hawk model

A nonlinear mathematical model was derived from a series of wind tunnel experiments and formulated by Davison[15]. The novel structure of the model allows it to capture, not only the lower angle of attack conventional pitch response of the model, but the departure at higher angles-of-attack to a stable large-amplitude limit-cycle regime and the bifurcations separating these regions. It was devised specifically to capture the variations in limit-cycle amplitude, frequencies and onset points, including multiple limit cycles where hysteresis occurs. Both the mathematical model (given in detail in Ref. 15), and the experimental rig upon which it is based represent a difficult control challenge to which eigenstructure assignment and dynamic gain scheduling have been applied, as well as other methods.

The nonlinear Hawk model was linearised into the following state-space form at each point for the DGS design:

$$\begin{bmatrix} \dot{q} \\ \dot{\theta} \end{bmatrix} = \begin{bmatrix} \left(M_q + M_{\dot{\alpha}}\right) & M_\alpha \\ 1 & 0 \end{bmatrix} \cdot \begin{bmatrix} q \\ \theta \end{bmatrix} + \begin{bmatrix} M_\eta \\ 0 \end{bmatrix} \cdot \eta \qquad \ldots (12)$$

where q (deg/s) is the pitch rate, θ (deg) is the pitch angle and η (deg) is the tailplane deflection angle. Note that for this experimental set-up, θ is equivalent to α. Coefficients M_q, M_α, $M_{\dot{\alpha}}$ and M_η were calculated by locally linearising the nonlinear mathematical model at a series of operating points along the trim curve.

4.2 Actuator modelling

In order to accurately model the experimental rig, it is important to include the dynamics of the actuator. The tailplane control surfaces used for actuation of the Hawk model in pitch exhibit various nonlinear effects such as a large deadband and rate limits. In order to be able to simulate this nonlinear behaviour the actuator dynamics were modelled and validated using experimental results by Davison[13]. The nonlinear model of the tailplane actuator from Ref. 13 is shown in Fig. 4.

This model was used for all the numerical simulations carried out and closely represents the dynamics of the real system. Using this nonlinear actuator model for control simulation, the expected closed-loop behaviour of the wind-tunnel model could be obtained prior to the test. It was necessary to use a linear approximation of the actuator model for control law design. Davison[13] derived the linear actuator model, shown in Equation (13), by comparing step responses with the full nonlinear model, to give a second-order transfer function.

$$\frac{\eta}{\eta_{dem}} = \frac{50,000}{s^2 + 1,250s + 50,000} \qquad \ldots (13)$$

5.0 OPEN-LOOP WIND-TUNNEL RESULTS

A slow ramp input was applied to the Hawk model in order to understand the steady-state response. Two sets of results were obtained; one for a ramp in h from +7 to –45 deg (Fig. 5) and the second for a ramp in h from –45 to +7 deg (Fig. 6). The ramp applied was gradual and it took over ten minutes to change the tailplane angle from one extreme to the other. These 'quasi-static' runs were used in order to extract 'experimental bifurcation diagrams'. Bifurcation diagrams show the variation of fixed points, or equilibria (i.e. points in state space where all time derivatives are zero), of a dynamic system (and their local stability) as a system parameter is varied. They have been used extensively for the analysis of nonlinear aircraft models[16-18].

The results shown in Figs 5 and 6 indicate a large amplitude limit cycle between η = –8° and η = +21°. Either side of this region, the responses represent equilibria, the oscillations being principally a result of the high turbulence level in the tunnel. The switch in behaviour topology at η = –8°, where the stable equilibria become unstable due to negative pitch damping and a stable limit cycle appears, is associated with a supercritical Hopf bifurcation. A comparison of Figs 5 and 6 indicates a region of hysteresis at tailplane angles between η = –16° and η = –21°, due

https://doi.org/10.1017/S0001924000004723 Published online by Cambridge University Press

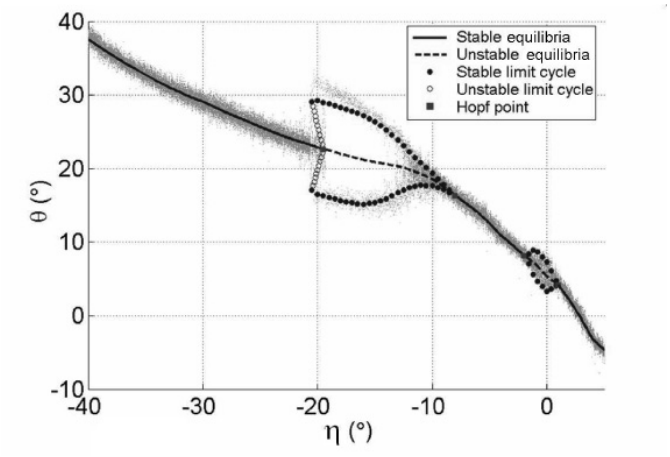


Figure 7. Uncontrolled Hawk: experimental and computed bifurcation diagrams.

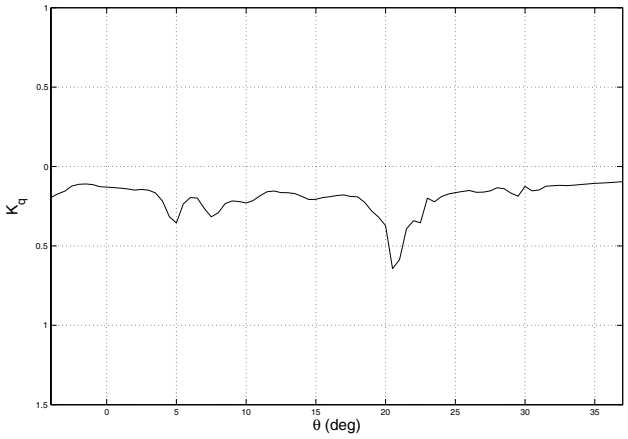


Figure 9. K_q: Static gain variation.

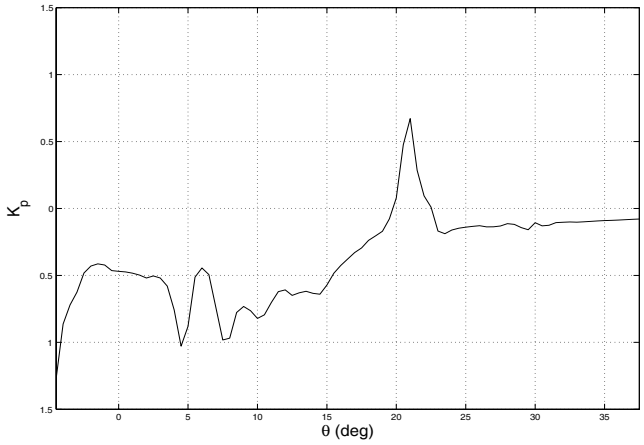


Figure 8. K_p: Static gain variation.

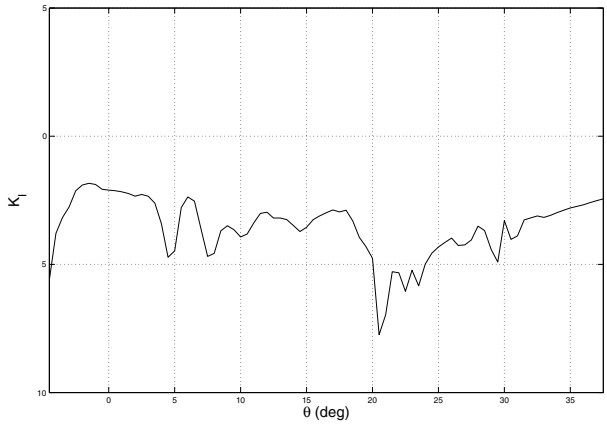


Figure 10. K_I: Static gain variation.

to a subcritical Hopf bifurcation at this end of the limit cycle region. The cause of this nonlinear behaviour is aerodynamic.

Figure 7 is a comparison between the mathematical model described in Section 4 and the experimental results. A bifurcation digram has been generated for the theoretical model and is shown to match the experimental results closely. Note also, the second small amplitude limit cycle present at low angles of θ, which is shown in the following section to correspond to rapid variation in required control system gains.

6.0 CLOSED-LOOP RESULTS

6.1 Gain schedules

The static gains, $\mathbf{K} = (K_p, K_I, K_q)$, were obtained using eigenstructure assignment applied to linearisations of the mathematical model at trim points for θ = –4·5° to 37·5° in steps of 0·5° and placement of the closed-loop eigenvalues at $\lambda_{short} = -5 \pm 5i$ for the short period mode and $\lambda_{int} = -6$ for the CAS integral mode.

Figure 8 shows the variation in the proportional gain against θ for the selected range (equivalent to a for this system). It can be seen that this variation is highly nonlinear, in particular in the region of θ = 20°, corresponding to the region of limit cycle hysteresis in the open loop model. There is also rapid variation in K_p in the region of θ = 5°, again corresponding to the small stable limit cycle at low angles-of-attack. This is unsurprising as it is in these regions where there is transition from stable to unstable behaviour for the trimmed branch of steady states, and the gains calculated are those which are required to provide a stable response from the Hawk throughout the desired θ range. Therefore, in these regions where there are rapid variations in the open loop eigenvalues and dynamic response there will be corresponding variations in required control system gains.

Figures 9 and 10 are the corresponding gains K_q and K_I required to give the desired dynamic response. They also show a nonlinear variation with θ and hence α. Moderate damping K_q is required throughout the range, with greater damping required in the limit cycle regions; a relatively large K_I is needed in order to obtain the desired dynamic response and closed loop poles.

Figure 11 shows the dynamic gain ϕ_p obtained from the transformation of K_p (Fig. 8) as laid out in the methodology in Section 2. Both static and dynamic proportional gains are shown.

https://doi.org/10.1017/S0001924000004723 Published online by Cambridge University Press

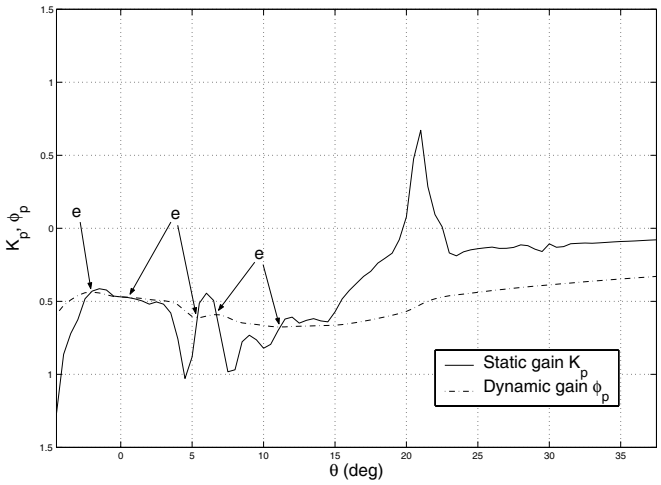


Figure 11. K_p and ϕ_p: Static and dynamic gain variation.

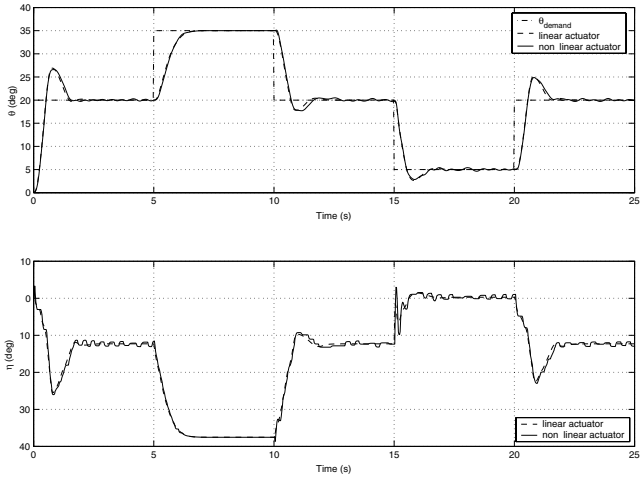


Figure 12. Simulation: response to a step input — CGS control.

It should be noted that the dynamic-gain variation is smooth and intersects the static-gain schedule at each point where the slope of $\phi(\theta) = 0$ (labelled with an *e* in Fig. 11) and at the point where θ is zero. This is a direct result of the transformation and is implicit within the equation used. There is also less variation in the dynamic gains when compared with the peaks and troughs evident in the static gains, especially at $\theta \approx 22°$.

This schedule, with the single state θ, accounts for the variation of the gain with a change in θ itself and therefore accounts for the hidden coupling term that would be present if a linearisation of the closed-loop system were taken. In an ideal case, each dynamic gain would be scheduled against each system state[2]. For example ϕ_p would be scheduled against θ, q and I, etc. (where I is the integrator state). It was found, however, that scheduling against a single state gave an acceptable response and so the complexity of scheduling against multiple states was not necessary. The decision to schedule all three gains with only a single state reduces the complexity of the system and in this case, has minimal effect on the dynamic performance of the closed-loop model.

For the following simulation and experimental tests, the term 'static gain schedule' implies use of the static gains K_p, K_q and K_I scheduled with the demanded input θ_{dem}. The term 'dynamic gain schedule' implies use of the dynamic gains, e.g. ϕ_p scheduled against the system

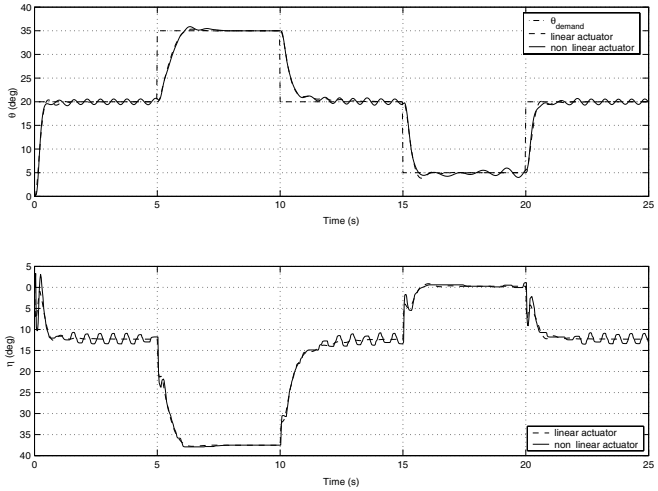


Figure 13. Simulation: response to a step input — DGS control.

state q. The static gains should, therefore, be correct for each linearisation of the closed-loop system and would (theoretically) give the desired response for small variations around a steady operating point.

For large variations in θ_{dem} the dynamic gain schedules should give a dynamic response closer to that of the desired eigenstructure. If the gains K were scheduled directly with the system state the hidden coupling terms mentioned in Section 2 could result in closed-loop system instability.

6.2 Simulation results

The first set of results shown here are simulations using the nonlinear mathematical model identified in Section 4 and the static and dynamic gains identified in Section 6.1. Figure 12 is a simulation of the step response of plus and minus 15 degrees demand from $\theta = 20$ degrees. Note that this region was selected due to the highly nonlinear behaviour present in the open-loop model. The gains used in this simulation were the static gains K scheduled with the input demand.

Figure 13 is the response of the system using dynamic gain scheduling. All three gains are scheduled against a single state, and are therefore set in real time, based on the current state of the system.

First of all, it should be noted that both systems are stable, showing well-behaved, well-damped system responses over this thirty degree range. The dynamic scheduled gains, however, show a more consistent dynamic response with a consistent overshoot in θ. The static scheduled response demonstrates variable dynamic properties with virtually no overshoot when stepping from 20 to 35 degrees and a relatively large overshoot when stepping from 5 to 20 degrees.

It is interesting to note the 2Hz oscillations which appear in both the CGS and DGS simulation results. Essentially these oscillations appear to be close in frequency to those of the limit cycle, and hence are likely to be aerodynamic in origin and are most evident within the limit cycle region. This is indeed the case, implying that the closed-loop controller does not fully damp out the limit cycle.

Two response lines are shown for both models, the second is for the system including the nonlinear actuator model in Fig. 4. This has a small oscillatory effect on the response but both systems are still stable. In summary, the simulation results show that dynamic gain scheduling results in a closed-loop response which is closer to the ideal given by the desired eigenstructure. This is most readily identified by the consistent overshoot in the DGS results. The difference arises from step changes in the static gains in a nonlinear region which are linked to θ_{dem}, and which, if scheduled directly with the system states, would result in undesired instability.

https://doi.org/10.1017/S0001924000004723 Published online by Cambridge University Press

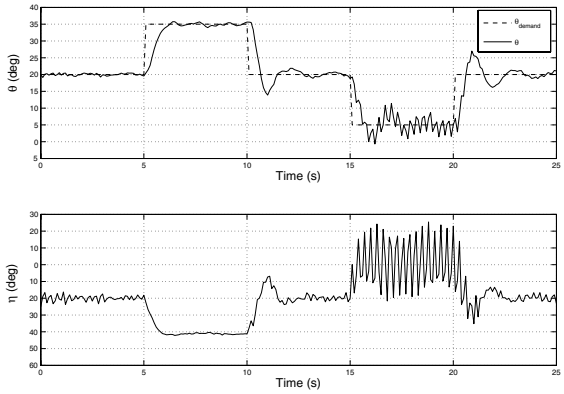


Figure 14. Experimental results: CGS step response.

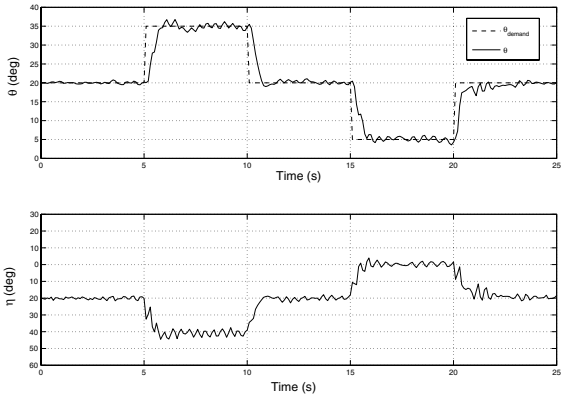


Figure 16. Experimental results: DGS step response.

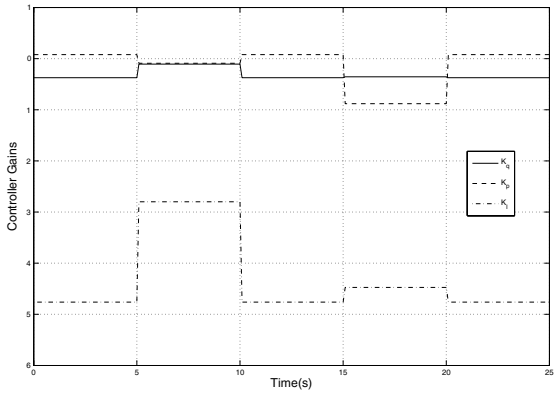


Figure 15. Experimental results: CGS gain variation.

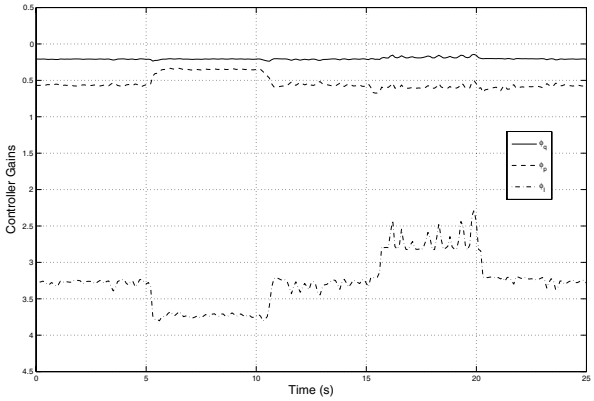


Figure 17. Experimental results: DGS gain variation.

6.3 Experimental results

Figures 14 and 16 demonstrate the difference in performance of the static (CGS) and dynamic (DGS) gain scheduled controllers. The experimental results show that the dynamic scheduled control system performs extremely well with step responses, having reduced overshoot, fast settling time and low control action. The system response was found to be stable at all operating points for the dynamic gain scheduled controller. In comparison, the static gain scheduled control system shown in Fig. 14 has a greater rise time, large overshoot and demonstrates a clear region of instability at low angles of attack, corresponding to the limit-cycle regions in Figs 5 and 6.

One of the advantages of dynamic gain scheduling is that the control system gains track the current state of the system. It should be noted at this point that both the static and dynamic scheduled controllers showed considerable improvement over simple fixed gain PID controllers, which were only suitable for very small regions of the desired operating range and which demonstrated instability over large regions. Other methods such as scheduled LQR gains and a form of adaptive control have also been applied, but to date, dynamic gain scheduling has been shown to give the best overall response.

Figures 15 and 17 show the corresponding variation in feedback gains for both the static and dynamic gain scheduled systems. Even though there is a fairly rapid variation in control system gains for the dynamic gain scheduled controller, the response shown in figure 16 is closer to the ideal. Note the smaller magnitude of the gains and the smooth transition between operating regions for the gains in the dynamic scheduled system.

Figures 18 and 19 show the response of both systems to a slow ramp input. As with the step response, an instability in the conventional gain scheduled system is evident in the vicinity of $\theta = 20$ degrees, which corresponds to the limit-cycle region evident in the uncontrolled aircraft. Note that no filtering of the aircraft sensors was carried out and no rate limits were placed on the actuator demands.

In Fig. 15 it is interesting to compare the two regions of instability with the experimental bifurcation results shown in Figs 5, 6 and 7, and to the variation in gains shown in Section 6.1. The instability of the steady states within both limit cycles, corresponds to rapid variations in the required static gains and to the two regions of instability which occur in the closed-loop ramp response at $\theta \approx 5$ degrees and $\theta \approx 20$ degrees. This seems to suggest that, not only do the dynamic gains give a better response to step changes in the demanded input, but they are more robust with respect to modelling uncertainties and nonlinearities in the open-loop system.

Both of these sets of results demonstrate that dynamic gain scheduling gives an improved dynamic response when compared with

https://doi.org/10.1017/S0001924000004723 Published online by Cambridge University Press

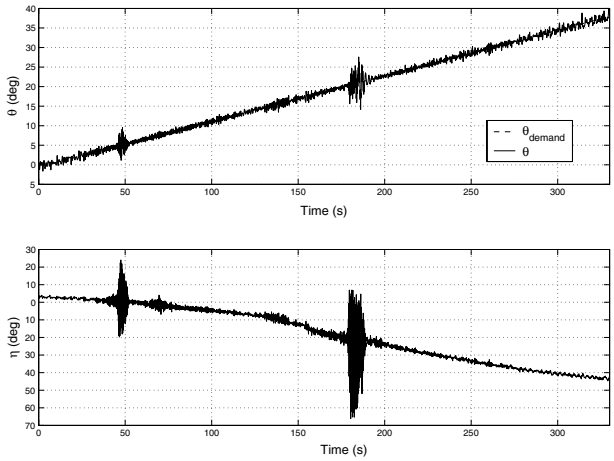


Figure 18. Experimental results: CGS ramp response.

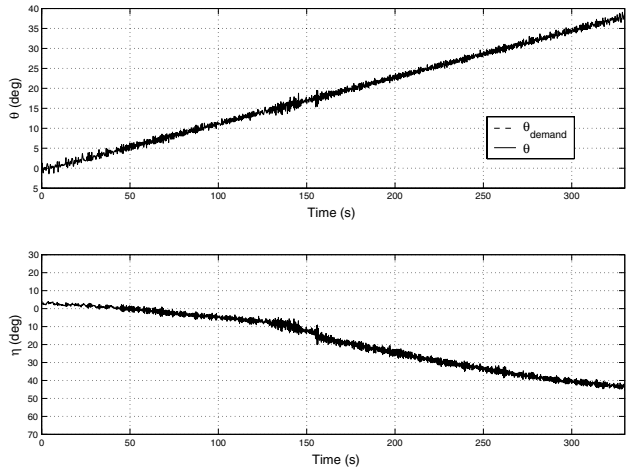


Figure 19. Experimental results: DGS ramp response.

conventional gain scheduled control systems. By allowing the user to schedule the control system gains with fast moving, highly coupled states, the control engineer is able to stabilise open-loop systems in regions which demonstrate highly nonlinear unstable open-loop behaviour. The dynamic gain scheduled approach is flexible, visible and effective, when applied to nonlinear systems such as aircraft operating at high angles-of-attack.

7.0 CONCLUSIONS

In this paper a method for scheduling state feedback gains against rapidly varying and coupled parameters, such as the system states, has been demonstrated on a highly nonlinear experimental aircraft rig. The method involves transforming the discrete parameter-dependent gain schedules (determined in this case by eigenstructure-based methods) into dynamic state-dependent schedules that are suitable for experimental implementation. This overcomes some of the limitations with previous gain-scheduled controllers which have constraints on the maximum rates of change of the scheduling parameter. Thus, even during transient motions, where rates of change of the states are large, the dynamic response of the system is improved.

This systematic approach to dynamic gain scheduling was applied to a single degree of freedom Hawk wind tunnel model and was shown to improve the dynamic response of the closed-loop system. With the dynamic gain scheduled control system, the experimental rig was stable over the entire operating range and exhibited acceptable transient behaviour. Moreover, the system demonstrated good turbulence rejection and acceptable robustness to actuator nonlinearities.

ACKNOWLEDGEMENTS

The authors are grateful to QinetiQ, Bedford, UK, for supporting the development of the pendulum support test rig.

REFERENCES

1. RUGH, W.J. and SHAMMA, J.S. Research on gain scheduling, *Automatica*, 2000, **36**, (10), pp 1401-1425.
2. RICHARDSON, T., DAVISON, P., LOWENBERG, M. and DI BERNARDO, M. Control of nonlinear aircraft models using dynamic state-feedback gain scheduling, August 2003, AIAA Paper, AIAA-2003-5503.
3. JONES, C.D.C., RICHARDSON, T.S. and LOWENBERG, M.H. Dynamic gain-scheduled control of the ICE 101-TV, *Aeronaut J*, December 2005, **109**, (1102), pp 593-607.
4. NICHOLS, R.A., REICHERT, R.T. and RUGH, W.J. Gain scheduling for H-infinity controllers: A flight control example, 1992, Technical report, John Hopkins University, Baltimore, MD.
5. JONES, C.D.C., RICHARDSON, T.S. and LOWENBERG, M.H. Dynamic state-feedback gain scheduled control of the ICE 101-TV, 2004, AIAA-2004-4754.
6. JONES, C.D.C., LOWENBERG, M.H. and RICHARDSON, T.S. Tailored dynamic gain-scheduled control. *J Guidance, Control and Dynamics*, 2006, **29**, (6), pp 1271-1281.
7. LIU, G.P. AND PATTON, R.J. *Eigenstructure Assignment for Control System Design*, 1998, John Wiley and Sons.
8. ANDRY, A.N., SHAPIRO, E.Y. and CHUNG, J.C. Eigenstructure assignment of linear systems. IEEE Transactions on Aerospace and Electronic Systems, 1983, **19**, (5), pp 711-728.
9. SOBEL, K.M., SHAPIRO, E.Y., and ANDRY, A.N. Eigenstructure assignment, *Int J Control*, 1994, 59, (1), pp 13-37.
10. JONES, C.D.C. Dynamic Gain-scheduled Control of a Nonlinear UCAV Model, 2006, PhD thesis, University of Bristol.
11. DUTTON, K., THOMPSON, S. and BARRACLOUGH, B. *The Art of Control Engineering*, 1998, Addison-Wesley.
12. COOK, M.V. *Flight Dynamics Principles*, 1997, Arnold.
13. DAVISON, P.M. Development, Modelling and Control of a Multi-degree-of-freedom Dynamic Wind Tunnel Rig, September 2003, PhD thesis, University of Bristol.
14. KYLE, H. An investigation into the use of a pendulum support rig for aerodynamic modelling, 2004, PhD thesis, University of Bristol.
15. DAVISON, P., LOWENBERG, M. and DI BERNARDO, M. Experimental analysis and modelling of limit cycles and bifurcations in a dynamic wind tunnel rig, *J Aircr*, July-August 2003, **40**, (4), pp 776-785.
16. LOWENBERG, M.H. Application of Bifurcation Analysis to Multiple Attractor Flight Dynamics, 1998, PhD thesis, University of Bristol.
17. LOWENBERG, M.H. Bifurcation analysis of multiple-attractor flight dynamics. *Philosophical Transactions of The Royal Society A: Mathematical, Physical and Engineering Sciences*, 1998, **356**, pp 2297-2319.
18. CARROLL, J.V. and MEHRA, R.K. Bifurcation analysis of nonlinear aircraft dynamics. *J Guidance, Control and Dynamics*, 1982, **5**, (5), pp 529-536.

https://doi.org/10.1017/S0001924000004723 Published online by Cambridge University Press